Article

A Galactic-scale gas wave in the solar neighbourhood

https://doi.org/10.1038/s41586-019-1874-z

Received: 20 June 2019

Accepted: 24 October 2019

Published online: 7 January 2020

João Alves[1,2*], Catherine Zucker[3], Alyssa A. Goodman[2,3], Joshua S. Speagle[3], Stefan Meingast[1], Thomas Robitaille[4], Douglas P. Finkbeiner[3,5], Edward F. Schlafly[6] & Gregory M. Green[7]

For the past 150 years, the prevailing view of the local interstellar medium has been based on a peculiarity known as the Gould Belt[1–4], an expanding ring of young stars, gas and dust, tilted about 20 degrees to the Galactic plane. However, the physical relationship between local gas clouds has remained unknown because the accuracy in distance measurements to such clouds is of the same order as, or larger than, their sizes[5–7]. With the advent of large photometric surveys[8] and the astrometric survey[9], this situation has changed[10]. Here we reveal the three-dimensional structure of all local cloud complexes. We find a narrow and coherent 2.7-kiloparsec arrangement of dense gas in the solar neighbourhood that contains many of the clouds thought to be associated with the Gould Belt. This finding is inconsistent with the notion that these clouds are part of a ring, bringing the Gould Belt model into question. The structure comprises the majority of nearby star-forming regions, has an aspect ratio of about 1:20 and contains about three million solar masses of gas. Remarkably, this structure appears to be undulating, and its three-dimensional shape is well described by a damped sinusoidal wave on the plane of the Milky Way with an average period of about 2 kiloparsecs and a maximum amplitude of about 160 parsecs.

To reveal the physical connections between clouds in the local interstellar medium (ISM), we determined the three-dimensional (3D) distribution of all local cloud complexes[11] by deriving accurate distances to about 380 lines of sight. The lines of sight were chosen to include not only all known local clouds[10,12] but also potential bridges between them, as traced by lower-column-density gas. Figure 1 presents the distribution of lines of sight studied towards the Galactic anti-centre and illustrates our overall approach. Each line of sight covers an area in the sky of about 450 arcmin^2 and includes both foreground and background stars for a particular direction towards a cloud. The distances and the colours of these stars are used to compute a distance to the cloud (see Methods).

In the interactive figure in Supplementary Information we present the distribution of cloud distances to all of the studied lines of sight in a Cartesian *XYZ* frame where *X* increases towards the Galactic centre, *Y* increases along the direction of rotation of the Galaxy and *Z* increases upwards out of the Galactic plane. In the *X*–*Y* projection (a top-down view of the Galactic disk), it is clear that cloud complexes are not randomly distributed, but instead tend to form elongated and relatively linear arrangements. Surprisingly, we find that one of the nearest structures, at about 300 pc from the Sun at its closest point, is exceptionally straight and narrow in the *X*–*Y* plane. This straight structure: (1) undulates systematically in the *Z* axis for about 2.7 kpc on the *X*–*Y* plane, (2) is co-planar in essentially its entire extent and (3) displays radial velocities[13] indicating that the structure is not a random alignment of molecular cloud complexes but a kinematically coherent structure. We find that this structure is well modelled as a damped sinusoidal wave. The red points in Fig. 2 were selected by the fitting procedure, by explicitly modelling inliers and outliers. We tested the validity of the model by modelling the 'tenuous connections' separately and confirming that they meet the same inlier criteria that were first applied to the major clouds. For more details on the statistical modelling, see Methods.

Apart from the continuous undulating 3D distribution, there is also very limited kinematic evidence that the structure is physically oscillating around the mid-plane of the Galaxy, as any sinusoidal mass distribution centred on the Galactic plane should. The Galactic space velocities (*U*, *V*, *W*) in the local-standard-of-rest frame for a sample of young stellar objects associated with the Orion A cloud near the 'trough" of this structure are (−10.2, −1.2, −0.1) km s^{-1} (J. Grossschedl, private communication), implying that Orion A has now reached its maximum distance from the Galactic plane before falling back into the plane. These observations also indicate that Orion, and probably the large structure described here, is moving tangentially with about the same speed as the local Galactic disk.

This spatially and kinematically coherent structure has an amplitude of roughly 160 pc at its maximum and a period of roughly 2 kpc. We estimate the mass of the structure to be at least $3 \times 10^6 M_\odot$ ($M_\odot$, solar mass) by integrating the Planck opacity map[14] for the different cloud complexes in the structure at their estimated distances. The procedures

[1]University of Vienna, Department of Astrophysics, Vienna, Austria. [2]Radcliffe Institute for Advanced Study, Harvard University, Cambridge, MA, USA. [3]Department of Astronomy, Harvard University and Center for Astrophysics, Harvard and Smithsonian, Cambridge, MA, USA. [4]Aperio Software, Leeds, UK. [5]Department of Physics, Harvard University, Cambridge, MA, USA. [6]Lawrence Berkeley National Laboratory, Berkeley, CA, USA. [7]Kavli Institute for Particle Astrophysics and Cosmology, Stanford University, Stanford, CA, USA. *e-mail: joao.alves@univie.ac.at

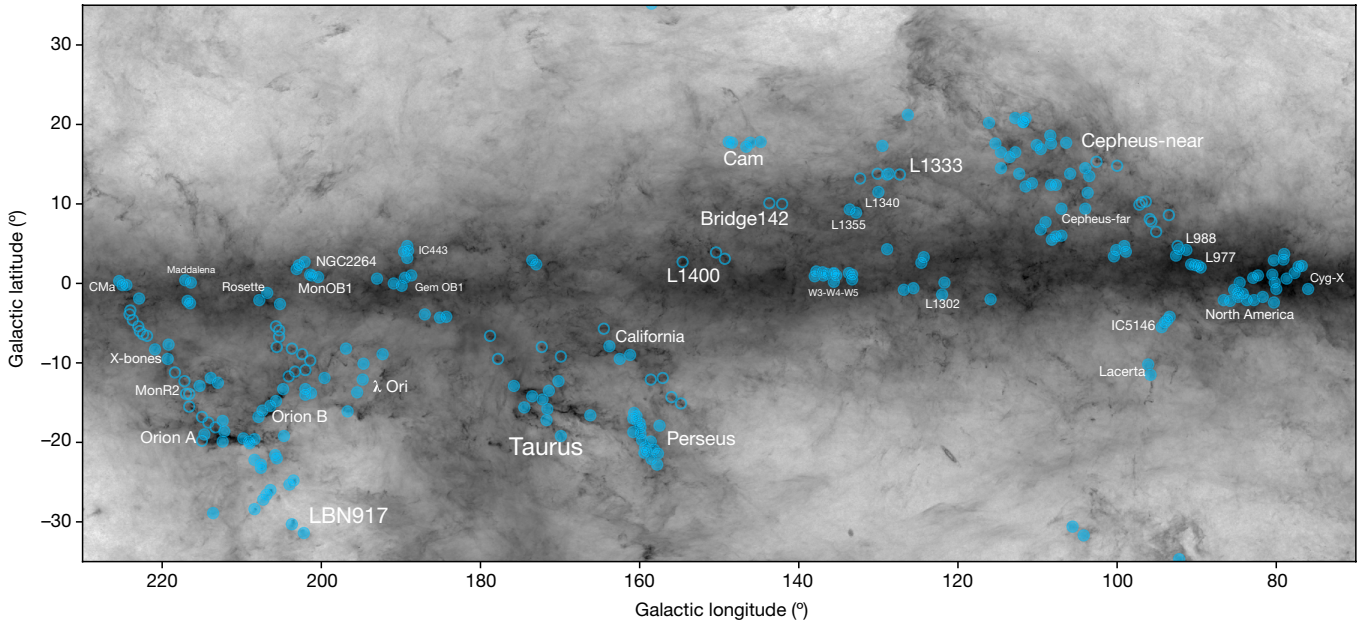

Fig. 1 | Sky map of targeted star-forming regions towards the anti-centre of the Milky Way. The filled circles represent the studied lines of sight used to determine accurate distances to known nearby star-forming complexes (the sizes of the region labels are roughly proportional to their distance). The open circles represent lines of sight towards lower-column-density envelopes between complexes. The background greyscale map shows the column density distribution derived from Planck data[14].

used to compute the mass and model the 3D shape of the structure are described in Methods. We name the structure the Radcliffe Wave in honour of both the early-20th-century female astronomers from Radcliffe College and the interdisciplinary spirit of the current Radcliffe Institute, which contributed to this discovery. The structure can also be seen at lower resolution in recent all-sky 3D dust maps[15–17] (see Fig. 2). A second linear structure, the 'split'[16], is about 1 kpc long and seems to contain the Sco-Cen, Aquila and Serpens clouds, as well as a previously unidentified complex. The functional form of the split is different, however, in that it is largely confined to the Galactic plane over much of its length and does not seem to be undulating.

The interactive figure in Supplementary Information, which displays the 3D location of the Gould Belt[18], illustrates that with the improved distances, this structure is a poor fit to the data, which comprise only clouds from Sco-Cen and Orion—the traditional anchors of the Gould Belt. This fact alone challenges the existence of a belt, as two points can

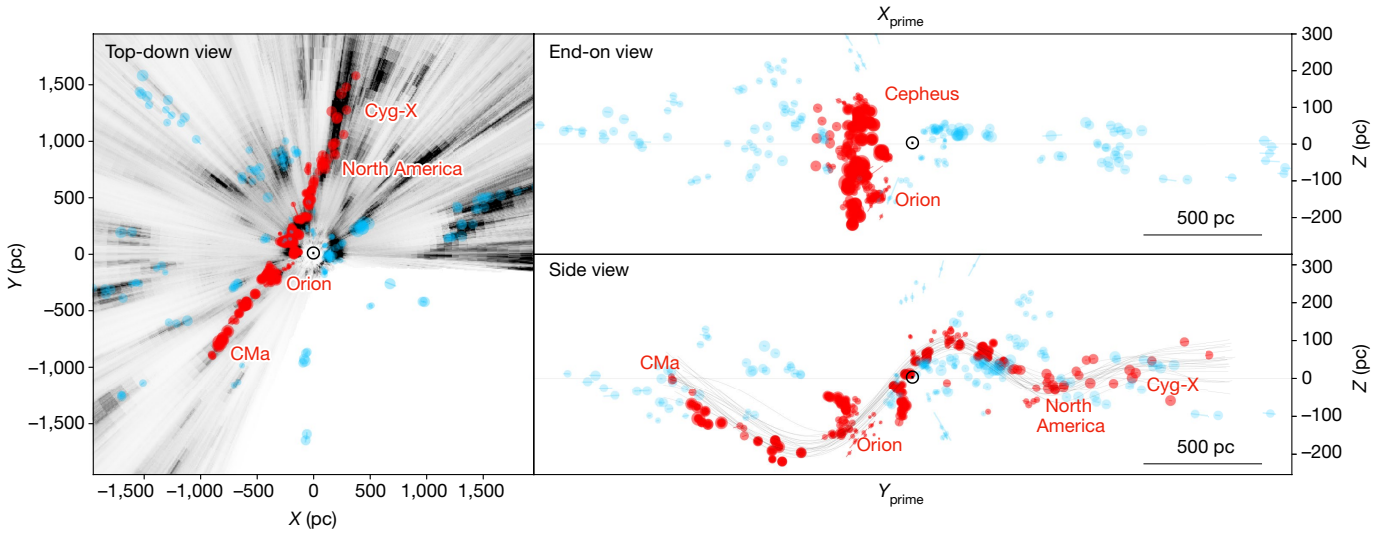

Fig. 2 | 3D distribution of local clouds. The position of the Sun is marked with ⊙. The size of the symbols is proportional to the column density. The red points were selected by a fitting algorithm, as described in Methods. These describe a spatially and kinematically coherent structure that we term the Radcliffe Wave (possible models are shown by the grey lines in the bottom-right panel). The greyscale map in the left panel show an integrated dust map[17] (−300 pc < Z < 300 pc), which indicates that our sample of cloud distances is essentially complete. To highlight the undulation and co-planarity of the structure, the right panels show projections in which the X–Y frame has been rotated anticlockwise by 33° (top, X_{prime}–Z) and clockwise by 120° (bottom, Y_{prime}–Z) for an observer facing the Galactic anti-centre. The 1σ statistical uncertainties on the distance (usually 1–2%) are represented by line segments that are usually smaller than the symbols. There is an additional systematic uncertainty on the distance, which is estimated[10] to be about 5%. For an interactive version of this figure, including additional layers not shown here (for example, a model of the Gould Belt and log-spiral arm fits), see Supplementary Information and https://faun.rc.fas.harvard.edu/czucker/Paper_Figures/radwave.html.

always define a ring. Because four out of five of the Gould Belt clouds (Orion, Perseus, Taurus, Cepheus) are part of the much larger Radcliffe Wave, whereas one of the five (Ophiuchus) is part of the split, we propose that the Gould Belt is a projection effect of two linear cloud complexes against the sky. Our results provide an alternate explanation for the 20° inclination of the Gould Belt: it is simply the orientation of the Radcliffe Wave from trough (Orion) to crest (Cepheus). With these considerations, the X–Y distribution of local B-stars in these regions from the 30-year-old Hipparcos satellite[19] resembles the two elongated linear structures in Fig. 2 more closely than a ring, bolstering previous suspicions that the Gould Belt is a projection effect[20].

In Supplementary Information, one can access an interactive display of the 3D location of the Local Arm of the Milky Way as traced by masers[21] and investigate the relation between the Radcliffe Wave and the Local Arm. The Radcliffe Wave (red points) is about 20% of the width and 40% of the length of the Local Arm[22] and makes up for an important fraction of the Local Arm's mass and number of cloud complexes. On the other hand, the Local Arm is much more dispersed and includes local complexes that are not part of the Radcliffe Wave (for example, Mon OB1, California, Cepheus Far and Ophiuchus). Whereas there is excellent agreement between our distance measurements and maser-defined distances[12], the log-spiral fit of the maser data crosses the Radcliffe Wave at an angle of about 25°. The mismatch between the Radcliffe Wave and the log-spiral fit suggests that the Local Arm is more structured and complex than previously thought, but is consistent with arms being composed of quasi-linear structures on kiloparsec scales[23,24].

The origin of the Radcliffe Wave is unclear. The structure is too large (and too straight) to have formed by the feedback of a previous generation of massive stars. More probably, this narrow structure is the outcome of a large-scale Galactic process of gas accumulation, either from a shock front in a spiral arm[25] or from gravitational settling and cooling on the plane of the Milky Way (Kim, W.-T. & Ostriker, E. C., manuscript in preparation). Linear kiloparsec-sized structures similar to the one presented here have been seen in nearby galaxies[26] and in numerical simulations[24] of spiral-arm formation.

The undulation of the Radcliffe Wave is even harder to explain. The accretion of a tidally stretched gas cloud settling into the Galactic disk could in principle mimic the shape and the damped undulation of the structure, but it requires synchronization with the Galactic rotation (Orion's velocity in the local-standard-of-rest frame, $V_{\rm LSR} \approx 0$ km s^{-1}), which is plausible but seems unlikely. Analogous kiloparsec-sized waves (or corrugations) have been seen in nearby galaxies[27] with amplitudes similar to the undulation seen in Fig. 2 (ref. [28]), but their origins often call for perturbers. Identifying possible disruption events, their corresponding progenitors and their relationship to the Radcliffe Wave is a substantial challenge that should be explored.

Our findings call for a revision of the architecture of gas in the solar neighbourhood and a re-interpretation of phenomena that are generally associated with the Gould Belt, such as the Lindblad ring and the Cas–Tau/α-Per populations, among many others[29]. The Radcliffe Wave provides a framework for understanding molecular cloud formation and evolution. Follow-up work, in particular on the kinematics of this structure, will provide insights into the relative roles of gravity, feedback and magnetic fields in star-formation research.

Online content

Any methods, additional references, Nature Research reporting summaries, source data, extended data, supplementary information, acknowledgements, peer review information; details of author contributions and competing interests; and statements of data and code availability are available at https://doi.org/10.1038/s41586-019-1874-z.

1. Herschel, J. F. W. *Results of Astronomical Observations Made During the Years 1834, 5, 6, 7, 8, at the Cape of Good Hope; Being the Completion of a Telescopic Survey of the Whole Surface of the Visible Heavens, Commenced in 1825* (Smith, Elder and Company, 1847).
2. Gould, B. A. On the number and distribution of the bright fixed stars. *Am. J. Sci.* **38**, 325–333 (1874).
3. Bobylev, V. V. The Gould belt. *Astrophysics* **57**, 583–604 (2014).
4. Palouš, J. & Ehlerová, S. in *Handbook of Supernovae* (eds Alsabti, A. W. & Murdin, P.) 2301–2311 (Springer, 2016).
5. Maddalena, R. J., Morris, M., Moscowitz, J. & Thaddeus, P. The large system of molecular clouds in Orion and Monoceros. *Astrophys. J.* **303**, 375–391 (1986).
6. Lombardi, M., Lada, C. J. & Alves, J. Hipparcos distance estimates of the Ophiuchus and the Lupus cloud complexes. *Astron. Astrophys.* **480**, 785–792 (2008).
7. Schlafly, E. F. et al. A large catalog of accurate distances to molecular clouds from ps1 photometry. *Astrophys. J.* **786**, 29 (2014).
8. Chambers, K. C. et al. *The Pan-STARRS1 surveys*. Preprint at https://arxiv.org/abs/1612.05560 (2016).
9. Brown, A. G. A., Vallenari, A., Prusti, T. & de Bruijne, J. H. J. Gaia Data Release 2: summary of the contents and survey properties. *Astron. Astrophys. Suppl. Ser.* **616**, A1 (2018).
10. Zucker, C. et al. A large catalog of accurate distances to local molecular clouds: the Gaia DR2 edition. *Astrophys. J.* **879**, 125 (2019).
11. Reipurth, B. (ed.) *Handbook of Star Forming Regions, Volume I: The Northern Sky* Vol. 4 (ASP, 2008).
12. Zucker, C. et al. A compendium of distances to molecular clouds in the star formation handbook. *Astron. Astrophys.* **633** A51 (2020).
13. Dame, T. M., Hartmann, D. & Thaddeus, P. The Milky Way in molecular clouds: a new complete CO survey. *Astrophys. J.* **547**, 792–813 (2001).
14. Planck Collaboration Planck 2013 results. XI. All-sky model of thermal dust emission. *Astron. Astrophys.* **571**, A11 (2014).
15. Green, G. M. et al. Galactic reddening in 3D from stellar photometry – an improved map. *Mon. Not. R. Astron. Soc.* **478**, 651–666 (2018).
16. Lallement, R. et al. Gaia-2MASS 3D maps of Galactic interstellar dust within 3 kpc. *Astron. Astrophys.* **625**, A135 (2019).
17. Green, G. M., Schlafly, E. F., Zucker, C., Speagle, J. S. & Finkbeiner, D. P. A 3D dust map based on gaia, Pan-STARRS 1 and 2MASS. *Astrophys. J* **887**, 93 (2019).
18. Perrot, C. A. & Grenier, I. A. 3D dynamical evolution of the interstellar gas in the Gould belt. *Astron. Astrophys. Suppl. Ser.* **404**, 519–531 (2003).
19. Elias, F., Cabrera-Caño, J. & Alfaro, E. J. OB stars in the solar neighborhood. I. Analysis of their spatial distribution. *Astron. J.* **131**, 2700–2709 (2006).
20. Bouy, H. & Alves, J. F. Cosmography of OB stars in the solar neighbourhood. *Astron. Astrophys. Suppl. Ser.* **584**, A26 (2015).
21. Reid, M. J., Dame, T. M., Menten, K. M. & Brunthaler, A. A parallax-based distance estimator for spiral arm sources. *Astrophys. J.* **823**, 77 (2016).
22. Reid, M. J. et al. Trigonometric parallaxes of high mass star forming regions: the structure and kinematics of the Milky Way. *Astrophys. J.* **783**, 130 (2014).
23. Honig, Z. N. & Reid, M. J. Characteristics of spiral arms in late-type galaxies. *Astrophys. J.* **800**, 53 (2015).
24. D'Onghia, E., Vogelsberger, M. & Hernquist, L. Self-perpetuating spiral arms in disk galaxies. *Astrophys. J.* **766**, 34 (2013).
25. Goodman, A. A. et al. The bones of the Milky Way. *Astrophys. J.* **797**, 53 (2014).
26. Elmegreen, B. G., Elmegreen, D. M. & Efremov, Y. N. Regularly spaced infrared peaks in the dusty spirals of Messier 100. *Astrophys. J.* **863**, 59 (2018).
27. Edelsohn, D. J. & Elmegreen, B. G. Corrugations in galactic discs generated by magellanic-type perturbers. *Mon. Not. R. Astron. Soc.* **287**, 947–954 (1997).
28. Matthews, L. D. & Uson, J. M. Corrugations in the disk of the edge-on spiral galaxy IC 2233. *Astrophys. J.* **688**, 237–244 (2008).
29. Bally, J. in *Handbook of Star Forming Regions* Vol. 4 (ed. Reipurth, B.) 459–370 (Astronomical Society of the Pacific, 2008).

Methods

Distances

Distances were determined for 326 lines of sight using major local molecular clouds and 54 'bridging' lines of sight in between molecular clouds coincident with the projected structure of the Radcliffe Wave. The methodology used to obtain the distances and the full catalogue of lines of sight for the major clouds are presented in complementary work[10,12]. Lines of sight for the major clouds were chosen to coincide with star-forming regions presented in ref. [11], which is considered to be the most comprehensive resource on individual low- and high-mass star-forming regions out to 2 kpc. Lines of sight for the tenuous connections were chosen in two dimensions to coincide with structures (for example, diffuse filamentary 'bridges'; see Fig. 1) that appeared to span the known star-forming regions on the plane of the sky without a priori knowledge of their distances. These were later used to validate the 3D modelling, which did not incorporate these distances.

Mass

We estimate the mass of the Radcliffe Wave to be about $3\times10^6 M_\odot$ using the Planck column density map shown in Fig. 1. To estimate the total mass, we first define the extent and depth for each complex in Fig. 1 using the information on the line-of-sight distances. We then integrate the column density map using the average distance to each complex. To correct for background contamination, which is critical for complexes closer to the plane, we subtract an average column density per complex estimated at the same Galactic latitude. Our resulting mass estimate of the Radcliffe Wave is probably an approximate lower limit to the true mass of the structure, given that the regions of the wave crossing the plane from Perseus to Cepheus and from Cepheus to Cygnus are poorly sampled owing to Galactic plane confusion.

Kinematics

We apply the open-source Gaussian fitting package PySpecKit[30] over local ^{12}CO spectral observations[13] to obtain the observed velocities of the star-forming regions shown in Extended Data Fig. 1. For each line of sight, we compute a spectrum over the same region that is used to compute the dust-based distances. We then fit a single-component Gaussian to each spectrum and assign the mean value as the velocity. We are not able to derive observed velocities for ~25% of the sample that either fall outside the boundaries of the survey[13], have no appreciable emission above the noise threshold and/or contain spectra that are not well modelled by a single-component Gaussian. The spectra that are not well modelled by a single-component Gaussian represent about 2% of the lines of sight and occur towards the most massive, structured and extinguished lines of sight in the sample, suggesting that these spectra could contain CO self-absorption features. We have confirmed that these more complex spectra do not show evidence of multiple distance components. Regardless, because the predicted velocities rely only on the estimated cloud distances assuming that they follow the 'universal' Galactic rotation curve[22], not every line of sight in Extended Data Fig. 1 has a corresponding observed velocity associated with its predicted velocity.

We compute the background greyscale map in Extended Data Fig. 1 by collapsing the ^{12}CO spectral observations over only the regions that are coincident with the cloud lines of sight on the plane of the sky.

3D modelling

We model the centre of the Radcliffe Wave using a quadratic function with respect to X, Y and Z specified by three sets of 'anchor points', (x_0, y_0, z_0), (x_1, y_1, z_1) and (x_2, y_2, z_2). We find that a simpler linear function is unable to accurately model the observed curvature in the structure and is subsequently disfavoured by the data.

The undulating behaviour with respect to the centre is described by a damped sinusoidal function relative to the X–Y plane with a decaying period and amplitude, which we parameterize as

$$\Delta z(t) = A \times \exp\left[-\delta\left(\frac{d(t)}{1\,\mathrm{kpc}}\right)^2\right] \times \sin\left[\left(\frac{2\pi d(t)}{P}\right)\left(1+\frac{d(t)/d_{\max}}{\gamma}\right)+\phi\right] \quad (1)$$

where $d(t) = \left\|(x,y,z)(t) - (x_0,y_0,z_0)\right\| = \sqrt{(x-x_0)^2+(y-y_0)^2+(z-z_0)^2}$ is the Euclidean distance from the start of the wave parameterized by t, $d_{\max}$ is the distance at the end of the wave, A is the amplitude, P is the period, ϕ is the phase, δ sets the rate at which the amplitude decays and γ sets the rate at which the period decays. We explored introducing an additional parameter to account for rotation around the primary axis determined by our quadratic fit, but found that the results were entirely consistent with the structure oscillating in the X–Y plane, and so excluded this parameter in our final model.

We assume the distance of each cloud d_{cloud} relative to our model to be normally distributed with an unknown scatter σ that is roughly equivalent to the radius of the wave. To account for different positions along the wave, we define this distance relative to the closet point as

$$d_{\mathrm{cloud}} = \min_t\left(\left\|(x_{\mathrm{cloud}}, y_{\mathrm{cloud}}, z_{\mathrm{cloud}}) - (x_{\mathrm{wave}}, y_{\mathrm{wave}}, z_{\mathrm{wave}})(t)\right\|\right) \quad (2)$$

Finally, we account for structure 'off' the wave by fitting a mixture model. We assume that a fraction f of clouds are distributed quasi-uniformly in a volume of roughly 10^7 pc^3, so that the remaining $1-f$ is part of the wave. We treat f entirely as a nuisance parameter because it is completely degenerate with the volume of our uniform outlier model, although we have specified it so that the uniform component will contribute a 'minority' of the fit (<40%).

Assuming that the distances to each of our n clouds have been derived independently, and defining $\theta = \{x_0, y_0, z_0, x_1, y_1, z_1, x_2, y_2, z_2, P, A, \phi, \gamma, \delta, \sigma, f\}$, the likelihood for a given realization of our 16-parameter 3D model is

$$\mathcal{L}(\theta) = \prod_{i=1}^{n}\left[(1-f)\mathcal{L}_{\mathrm{cloud},i}(\theta) + f\mathcal{L}_{\mathrm{unif},i}(\theta)\right] \quad (3)$$

where

$$\mathcal{L}_{\mathrm{cloud},i}(\theta) = \frac{1}{\sqrt{2\pi\sigma^2}}\exp\left[-\frac{1}{2}\frac{d_{\mathrm{cloud},i}^2}{\sigma^2}\right]$$
$$\mathcal{L}_{\mathrm{unif},i}(\theta) = 10^{-7} \quad (4)$$

We infer the posterior probability distribution $\mathcal{P}(\theta)$ of the 3D model parameters to be consistent with our cloud distances (excluding all bridging features) using Bayes' theorem:

$$\mathcal{P}(\theta) \propto \mathcal{L}(\theta)\pi(\theta) \quad (5)$$

where $\pi(\theta)$ is our prior distributions over the parameters of interest. We set our prior $\pi(\theta)$ to be independent for each parameter, on the basis of initial fits. The priors on each parameter are described in Extended Data Table 1, where $\mathcal{N}(\mu, \sigma)$ is a normal distribution with mean μ and standard deviation σ and $\mathcal{U}(a, b)$ is a uniform distribution with lower bound a and upper bound b.

We generate samples from $\mathcal{P}(\theta)$ with the nested sampling code dynesty[31] using a combination of uniform sampling with multi-ellipsoid decompositions and 1,000 live points. A summary of the derived properties of the Radcliffe Wave are listed in Extended Data Table 2 along with their associated 95% credible intervals. The 20 random samples from $\mathcal{P}(\theta)$ are plotted in Fig. 2 to illustrate the uncertainties in our model.

Using our samples, we associate particular sightlines with the Wave by computing the mean odds ratio averaged over our posterior

$$\langle R_i \rangle = \int \frac{(1-f)\mathcal{L}_{\mathrm{cloud},i}(\theta)}{f\mathcal{L}_{\mathrm{unif},i}(\theta)} \mathcal{P}(\theta) \mathrm{d}\theta \quad (6)$$

based on our set of samples. We subsequently classify all objects with $\langle R_i \rangle > 1$ as being part of the Radcliffe Wave, which is used as the criterion for associating sources in Fig. 2. We find that this condition holds true for 43% of the sources used to determine our initial model. Our overall conclusions do not change if larger, more selective thresholds are chosen.

As further validation, we subsequently compute $\langle R_i \rangle$ for each of the 54 bridging lines of sight targeted to follow the projected structure of the Radcliffe Wave. We find that all 54 lines of sight satisfy our $\langle R_i \rangle > 1$ condition, further confirming the continuous nature of the Wave between individual clouds.

In addition to the parameters derived above, we estimate the total length of the feature in our dataset by computing the line integral along our model from the clouds at the endpoints, finding a length of 2.7 ± 0.2 kpc (95% credible interval). The derived physical properties of the feature are listed in Extended Data Table 3.

Data availability

The datasets generated and/or analysed during the current study are publicly available on the Harvard Dataverse: the distances to the major star-forming clouds are available at https://doi.org/10.7910/DVN/07L7YZ and the tenuous connections at https://doi.org/10.7910/DVN/K16GQX.

Code availability

The software used to determine the distances to star-forming regions is publicly available on Zenodo (https://doi.org/10.5281/zenodo.3348370 and https://doi.org/10.5281/zenodo.3348368). The code used for model fitting is available from J.S.S. (jspeagle@cfa.harvard.edu) on reasonable request.

30. Ginsburg, A. PySpecKit: Python spectroscopic toolkit. Astrophysics Source Code Library ascl:1109.001 (2011).
31. Speagle, J.S. *dynesty: a dynamic nested sampling package for estimating Bayesian posteriors and evidences*. Preprint at https://arxiv.org/abs/1904.02180 (2019).

Acknowledgements J.A. thanks the Radcliffe Institute, where this work was developed, and where J.A. discovered the work of visual artist A. von Mertens on H. Leavitt's work, which inspired us to "see more". We acknowledge the organizers and participants of the 'The Milky Way in the age of Gaia' workshop of the 2018 Paris-Saclay International Programs for Physical Sciences, as well as the Interstellar Institute, for discussions at the early stage of this work. We benefited from discussions with T. Dame, M. Reid, A. Burkert and M. Davies. J.A. acknowledges the TURIS and Data Science Research Platforms of the University of Vienna. C.Z. and J.S.S. are supported by the NSF Graduate Research Fellowship Program (grant number 1650114) and the Harvard Data Science Initiative. D.P.F. and C.Z. acknowledge support by NSF grant AST-1614941. E.F.S. acknowledges support by NASA through ADAP grant NNH17AE75I and Hubble Fellowship grant HST-HF2-51367.001-A awarded by the Space Telescope Science Institute, which is operated by the Association of Universities for Research in Astronomy, Inc., for NASA, under contract NAS 5-26555. The computations in this paper used resources from the Odyssey cluster, which is supported by the FAS Division of Science Research Computing Group at Harvard University. The high-dimensional visualization software Glue, which was used to explore, visualize and understand the Radcliffe Wave, was created by A.A.G., T.R., C.Z. and others, and has been supported by US Government contract NAS5-03127 through NASA's James Webb Space Telescope Mission and NSF awards OAC-1739657 and AST-1908419. We are grateful to A. Johnson and others at Plotly Graphing Library for their help creating the 3D interactive figure, which was output from Glue to Plotly. WorldWide Telescope (WWT), which was used within Glue to visualize the wave, is currently supported by NSF grant 1642446 to the American Astronomical Society. WWT was originally created by C. Wong and J. Fay at Microsoft Research, which supported WWT development before the American Astronomical Society. J.S.S. thanks R. Bleich, and J.A. thanks A. dell'Erba, J. Alves, M. Alves and R. Alves for continuing support.

Author contributions J.A. led the work and wrote most of the text. All authors contributed to the writing of the manuscript. C.Z. and J.S.S. led the data analysis and distance modelling with E.F.S., G.M.G. and D.P.F. C.Z. and J.A. led the kinematics analysis. J.A., C.Z. and A.A.G. led the visualization efforts. J.S.S. led the 3D modelling. J.A., C.Z. and A.A.G. led the efforts to interpret the results. T.R., A.A.G., J.S.S. and C.Z. contributed to the development of the software used in this work.

Competing interests The authors declare no competing interests.

Additional information
Supplementary information is available for this paper at https://doi.org/10.1038/s41586-019-1874-z.
Correspondence and requests for materials should be addressed to J.A.
Reprints and permissions information is available at http://www.nature.com/reprints.

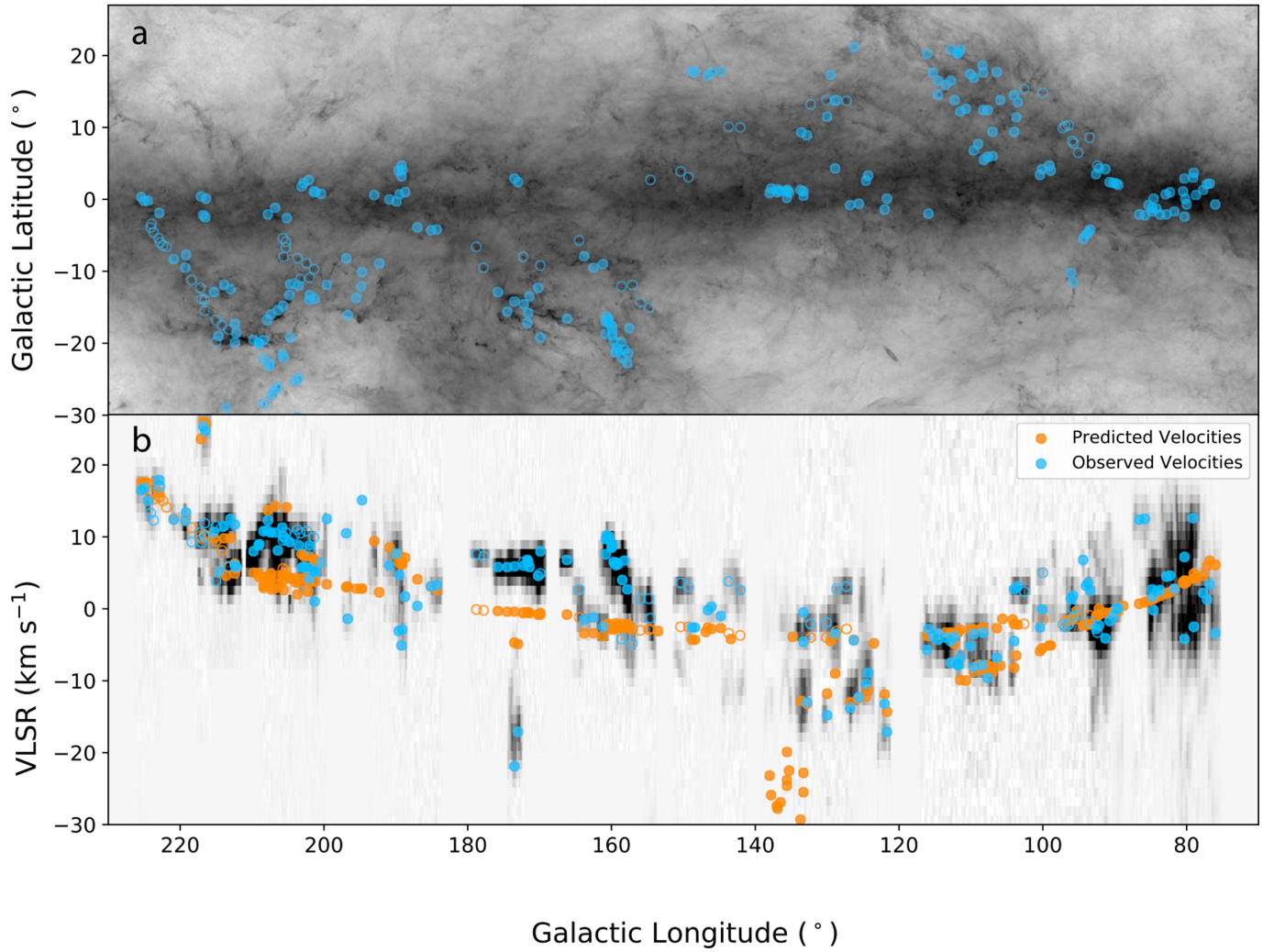

Extended Data Fig. 1 | Position–velocity diagram. a, **b**, The blue points in **a** are as in Fig. 1 and the orange points in **b** represent the predicted positions of the blue points as if they were following a 'universal' Galactic rotation curve[22]. The line segments represent 1σ errors, derived from a Gaussian fitting for the observed velocities and the distance uncertainties for the predicted velocities, and are generally smaller than the symbols. The quasi-linear arrangement in velocity of the Radcliffe Wave complexes suggests that the structure is not a random alignment of molecular cloud complexes, but a kinematically coherent structure. The tentative decoupling between observed and predicted velocities also indicate that the Radcliffe Wave is a kinematically coherent structure. VLSR, velocity in the local-standard-of-rest frame.

Extended Data Table 1 | Priors on Radcliffe Wave parameters

Parameter	Prior
x_0	$\mathcal{N}(-900\,\mathrm{pc}, 100\,\mathrm{pc})$
y_0	$\mathcal{N}(-900\,\mathrm{pc}, 100\,\mathrm{pc})$
z_0	$\mathcal{N}(0\,\mathrm{pc}, 50\,\mathrm{pc})$
x_1	$\mathcal{N}(-300\,\mathrm{pc}, 100\,\mathrm{pc})$
y_1	$\mathcal{N}(0\,\mathrm{pc}, 100\,\mathrm{pc})$
z_1	$\mathcal{N}(0\,\mathrm{pc}, 50\,\mathrm{pc})$
x_2	$\mathcal{N}(300\,\mathrm{pc}, 100\,\mathrm{pc})$
y_2	$\mathcal{N}(1400\,\mathrm{pc}, 100\,\mathrm{pc})$
z_2	$\mathcal{N}(0\,\mathrm{pc}, 50\,\mathrm{pc})$

Parameter	Prior
P	$\mathcal{N}(3500\,\mathrm{pc}, 300\,\mathrm{pc})$
A	$\mathcal{N}(170\,\mathrm{pc}, 20\,\mathrm{pc})$
ϕ	$\mathcal{N}(2.9\,\mathrm{rad}, 0.5\,\mathrm{rad})$
$\ln\gamma$	$\mathcal{N}(-0.5, 0.5)$
$\ln\delta$	$\mathcal{N}(-0.5, 0.5)$
$\ln\sigma/\mathrm{pc}$	$\mathcal{U}(3.5, 5)$
f	$\mathcal{U}(0.15, 0.4)$

Extended Data Table 2 | Constraints on Radcliffe Wave parameters

Parameter	Median with 95% CI	Parameter	Median with 95% CI
x_0	-910^{+130}_{-150} pc	P	3560^{+500}_{-470} pc
y_0	-860^{+140}_{-130} pc	A	160^{+30}_{-30} pc
z_0	-30^{+80}_{-80} pc	ϕ	$2.89^{+0.51}_{-0.58}$ rad
x_1	-270^{+80}_{-80} pc	γ	$0.50^{+0.27}_{-0.17}$
y_1	-20^{+160}_{-150} pc	δ	$6.68^{+5.48}_{-3.20}$
z_1	-10^{+30}_{-30} pc	σ	62^{+16}_{-13} pc
x_2	290^{+70}_{-70} pc	f	$0.22^{+0.07}_{-0.06}$
y_2	1400^{+170}_{-170} pc		
z_2	30^{+50}_{-50} pc		

CI, credible interval.

Extended Data Table 3 | Physical properties of the Radcliffe Wave

Name	Median with 95% CI
Length	2.7 ± 0.2 kpc
Scatter	60 ± 15 pc
Amplitude	160 ± 30 pc
Mass	$\geq 3 \times 10^6$ $M_\odot$